JACS
JOURNAL OF THE AMERICAN CHEMICAL SOCIETY
Article
pubs.acs.org/JACS

Al_2O_3 Surface Complexation for Photocatalytic Organic Transformations

Wan Ru Leow,[†] Wilson Kwok Hung Ng,[‡] Tai Peng,[†] Xinfeng Liu,[‡] Bin Li,[†] Wenxiong Shi,[†] Yanwei Lum,[§,∥] Xiaotian Wang,[†] Xianjun Lang,[†] Shuzhou Li,[†] Nripan Mathews,[†] Joel W. Ager,[§,∥] Tze Chien Sum,[‡] Hajime Hirao,*[,‡] and Xiaodong Chen*[,†]

[†]Innovative Center for Flexible Devices, School of Materials Science and Engineering, Nanyang Technological University, 50 Nanyang Avenue, Singapore 639798

[‡]School of Physical and Mathematical Sciences, Nanyang Technological University, 21 Nanyang Link, Singapore 637371

[§]Joint Center for Artificial Photosynthesis, Materials Sciences Division, Lawrence Berkeley National Laboratory, Berkeley, California 94720, United States

[∥]Department of Materials Science and Engineering, University of California, Berkeley, California 94720, United States

Supporting Information

ABSTRACT: The use of sunlight to drive organic reactions constitutes a green and sustainable strategy for organic synthesis. Herein, we discovered that the earth-abundant aluminum oxide (Al_2O_3) though paradigmatically known to be an insulator could induce an immense increase in the selective photo-oxidation of different benzyl alcohols in the presence of a large variety of dyes and O_2. This unique phenomenon is based on the surface complexation of benzyl alcohol (BnOH) with the Brønsted base sites on Al_2O_3, which reduces its oxidation potential and causes an upshift in its HOMO for electron abstraction by the dye. The surface complexation of O_2 with Al_2O_3 also activates the adsorbed O_2 for receiving electrons from the photoexcited dyes. This discovery brings forth a new understanding on utilizing surface complexation mechanisms between the reactants and earth abundant materials to effectively achieve a wider range of photoredox reactions.

1. INTRODUCTION

Photoredox catalysis has great potential in facilitating organic transformations to valuable products,[1,2] as it is environmentally friendly, cost-effective, and easily realized by mere household fixtures. Therefore, much research has been conducted on photoabsorbing molecules and complexes to convert solar energy to chemical energy.[3] Out of these, Ru-based polypyridyl complexes have attracted immense popularity due to their ease of synthesis, stability, and good photoredox capabilities.[4,5] Recently, the merging of photocatalysis and other types of catalysis, e.g., organocatalysis[6,7] and nickel[8,9] or gold[10,11] catalysis, could enable a large variety of difficult organic transformations[1,12,13] such as the coupling of aryl halides with amino acids,[8] tertiary anilines,[14,15] carboxylic acids,[16] organoborates,[9,17,18] and α-oxo acids.[19] Meanwhile, selective oxidation constitutes a class of difficult organic transformation, e.g., the oxidation of benzyl alcohols to aldehydes[20−23] and sulfides to sulfoxides,[24,25] which is essential for converting raw materials into fine chemicals especially in the flavor and fragrance industry.[20,24,26] The typical synthesis route requires toxic oxidants that are detrimental to health and the environment.[27−30] As for the photocatalytic redox route, the reaction can proceed only if the redox potential of the photocatalyst is greater than that of the reactants.[3] Conventional strategies to fulfill this condition include using wide band gap semiconductors[31] such as TiO_2[20,24] or Nb_2O_5[32] and modifying the cation[3,33,34] or ligands of transition metal complexes to tune the redox potential.[3,35] However, the former method can only utilize the short wavelength range of the solar spectrum, while the latter requires unique photocatalysts to be synthesized for specific reactions.

In the past development of photocatalysis, aluminum oxide (Al_2O_3) has played a supporting rather than a central role, serving as high surface area supports and photochemically inert barriers.[36,37] This is because alumina is an electrical insulator with a wide band gap of 8.7 eV.[38] However, Al_2O_3, in particular the γ-phase, possesses unique surface properties such as bifunctional Brønsted and Lewis acid and base sites,[39,40] which can endow supported materials with catalytic activity that is absent in the pristine materials.[41,42] Examples include Ag/Al_2O_3 for enhanced NO reduction[43,44] and V_2O_5/Al_2O_3 for the photo-oxidation of cyclohexane.[45] Thus, we propose that the redox potentials of organic reactants can be modified through surface complexation with Al_2O_3, which can be coupled with photocatalysis to facilitate demanding organic transformations under mild conditions.

Received: October 5, 2016
Published: December 14, 2016

DOI: 10.1021/jacs.6b09934
J. Am. Chem. Soc. 2017, 139, 269−276

In this article, we report that Al_2O_3 surface complexation can enable the highly selective oxidation of benzyl alcohols to benzaldehydes in the presence of dye, O_2, and visible light, even though negligible oxidation occurred with the dye alone. This phenomenon can be extended to dyes of different moieties. The underlying mechanism is that the oxidation potential of benzyl alcohol may be decreased through simple complexation with Al_2O_3, thus rendering it susceptible to oxidation by photocatalysts with smaller redox potentials. The complexation of O_2 with Al_2O_3 also enables it to receive electrons from the photoexcited dye, thus facilitating the overall transfer of protons and electrons from benzyl alcohol to O_2. This method would bring forth the potential of utilizing surface complexation mechanisms between the reactants and earth abundant materials to achieve a wider range of photoredox reactions.

2. MATERIALS AND METHODS

2.1. Preparation and Characterization of Al_2O_3. All solid catalysts were purchased from Sigma-Aldrich and Alfa Aesar and used without further modification. The synthesized Al_2O_3 was prepared by solid state reaction, in which 7.5 g of aluminum nitrate nonahydrate ($Al(NO_3)_3{\cdot}9H_2O$) dissolved in 50 mL of deionized water was adjusted to pH 7.0 with $NH_3{\cdot}H_2O$ solution, dried, and then calcined at 600 °C.

Powder X-ray diffraction (XRD) was recorded by a Bruker-AXS X-ray diffractometer with Cu Kα irradiation (λ = 1.5418 Å). The morphologies of the samples were examined by scanning (SEM, JEOL-JSM-7600F) and high-resolution transmission electron microscopy (HRTEM, JEOL-JEM-2100F). The Brunauer–Emmett–Teller (BET) surface area was measured with an ASAP 2020 apparatus (Micromeritics Instrument Corp.). UV–visible diffuse reflectance spectroscopy was used to measure the optical properties of Al_2O_3 with barium sulfate as the reference and transformed to the absorption spectra according to the Kubelka–Munk relationship. The CO_2-TPD was performed on the Auto Chem 2920 (USA) apparatus. A 0.10 g amount of the sample was loaded in a U-shaped quartz tube, heated at 550 °C for 1 h in helium flow, and then cooled to 40 °C in order to saturate the sample with CO_2. The CO_2-TPD spectrum was then measured in the temperature range of 40–600 °C at a constant heating rate of 10 °C min^{-1}. X-ray photoelectron spectroscopy (XPS) was performed using a Kratos Axis Ultra DLD system with a monochromatized Al Kα source ($h\nu$ = 1486.6 eV). A takeoff angle of 0° relative to the surface normal was used to sample the maximum surface depth. The subsequent XPS peak fitting and analysis were performed with the CasaXPS software. Energy calibration was referenced to the C 1s peak at 284.8 eV. Fourier transform infrared (FTIR) spectroscopy was performed on the Al_2O_3 samples pelletized with KBr using a PerkinElmer Frontier setup.

2.2. Reaction and Postreaction Analysis. All reactants and catalysts were purchased from Sigma-Aldrich and Alfa Aesar and used without further purification, while all solvents were purchased from Fisher Chemical. The solid catalysts were thermally pretreated at 200 °C under ambient atmosphere prior to reaction to remove surface water and impurities. In a typical reaction, 50 mg of Al_2O_3, 0.5 μmol of $Ru(bpy)_3Cl_2$, and 0.1 mmol of BnOH were added to 5 mL of CH_3CN in a Pyrex vessel and allowed to stir for 30 min in the dark. O_2 was then purged into the Pyrex vessel to achieve an O_2 atmosphere of pressure 0.1 MPa. The reaction mixture was then illuminated by the 7 W white light household LED, the irradiating wavelength range of which was measured to be 400–700 nm, with two maxima at 450 and 550 nm (Figure S10a), under magnetic stirring at 800 rpm.

Upon reaction completion, Al_2O_3 was separated from the reaction mixture by centrifugation. The collected Al_2O_3 was washed twice with CH_3CN and dried overnight in a vacuum oven at 60 °C prior to characterization. The product identities were confirmed by comparison of the gas chromatography (GC) retention times with that of standard samples. The products were then quantitatively analyzed through a GC (Agilent 7890A) equipped with a flame ionization detector (FID) and Agilent Technology 19091J-413 capillary column (30 m × 0.32 mm × 0.25 mm) using high-purity N_2 as the carrier gas and chlorobenzene as the internal standard. The standard analysis conditions are as follows: injector temperature 250 °C, detector temperature 300 °C, and column temperature ramped from 50 to 300 °C with a rate of 20 °C min^{-1}. GC–MS analysis was conducted with a Shimadzu GC 2010 gas chromatograph equipped with a Shimadzu GCMSQP2010 Ultra mass spectrometer and a Restek (Rxi-5Sil MS) capillary column (30 m × 0.25 mm × 0.25 mm), coupled with an electron ionization mass spectrometer with high-purity He as the carrier gas.

2.3. Cyclic Voltammetry. The Al_2O_3-modified electrode was fabricated according to procedures present in literature. Basically, Al_2O_3 paste was deposited using the doctor-blade technique on fluorine-doped stannic oxide coated glass (sheet resistance of 15 Ω/sq, Nippon Sheet Glass Co., Ltd., Japan). The resultant layer was dried in air at room temperature and heated at 450 °C for 1 h before cooling to room temperature.

Cyclic voltammetry was carried out using a CHI 660D electrochemical workstation (CH Instruments, Inc., Austin, USA). A three-electrode configuration was used for the measurement of cyclic voltammetry. We used Al_2O_3-modified FTO glass as the working electrode, a Pt wire as the counter electrode, and an Ag/Ag^+ electrode as the reference. A 0.1 M solution of tetra-*n*-butylammonium hexafluorophosphate (TBAPF6) in CH_3CN was used as the supporting electrolyte. Ferrocene was employed as internal standard. A glassy carbon electrode was used as working electrode for the measurement of oxidative potential of BnOH.

2.4. Theoretical Simulation of the BnO–Al_2O_3 Surface Complex and Dyes' Energy Structure. All calculations are based on the Al_2O_3 model proposed by Digne et al.[46] A slab with the (110) facet exposed and dimensions of (16.826 Å × 16.136 Å × 25.000 Å) is created to model the BnOH adsorption, while the periodic boundary condition calculations were conducted with VASP computational packages.[47−50] The PBE functional and PAW method were used for calculation, and only the Γ point is chosen for Brillouin zone sampling.[51−53] An isolated complex was used to describe the BnO–Al_2O_3 surface complex approximately, and it was assumed that neighboring BnOH, $Ru(bpy)_3^{2+}$, and solvent molecules do not exert a large influence on its energy levels. The HOMO level of the free BnOH molecule is determined from the vertical ionization energy, which is calculated by the Gaussian09 package using the PBE functional with 6-31+G* basis set. The vacuum level is used to locate the absolute energy level.

The Gaussian09 package was used for the DFT calculation of the dye molecules. The B3LYP functional with 6-31G* basis set is used for the calculations. For Rose Bengal, the iodide atoms were treated with the SDD basis set. To take the solvation effect into account, the self-consistent reaction field (SCRF) approach was used, and the solvent involved is acetonitrile.[51−53] The energy level of Rhodamine B in vacuum is very low due to its positive charge (no counterion is added to the system). The HOMO–LUMO gaps are almost always larger that the S_0S_1 transition energy predicted by TDDFT. This is the most significant for $Ru(bpy)_3^{2+}$ as it is cationic and its electronic transition is MLCT, which tends to deviate a lot from its HOMO–LUMO gap.

2.5. Time-Resolved Photoluminescence (TRPL). A pump wavelength of 400 nm was used for the TRPL measurements, which originates from the frequency-doubled 800 nm laser pulses generated from a Coherent Libra Regenerative Amplifier using a Beta Barium Borate (BBO) crystal. The luminescence signal was collected and then dispersed by a DK240 1/4-m monochromator with 300 g mm^{-1} grating. The transient photoluminescence signal was resolved by an Optronis Optoscope streak camera system, which possesses an ultimate temporal resolution of about 10 ps when operated at the fastest scan speed.

3. RESULTS AND DISCUSSION

First, a series of different benzyl alcohols, **1a–k**, was tested with $Ru(bpy)_3^{2+}$ as the photosensitizer and mild conditions such as irradiation with a 7 W household white light LED and O_2 as the

DOI: 10.1021/jacs.6b09934
J. Am. Chem. Soc. 2017, 139, 269–276

oxidant (Figure 1a). The Al_2O_3 used is the commercially available Aldrich 517747, unless otherwise stated. XRD studies

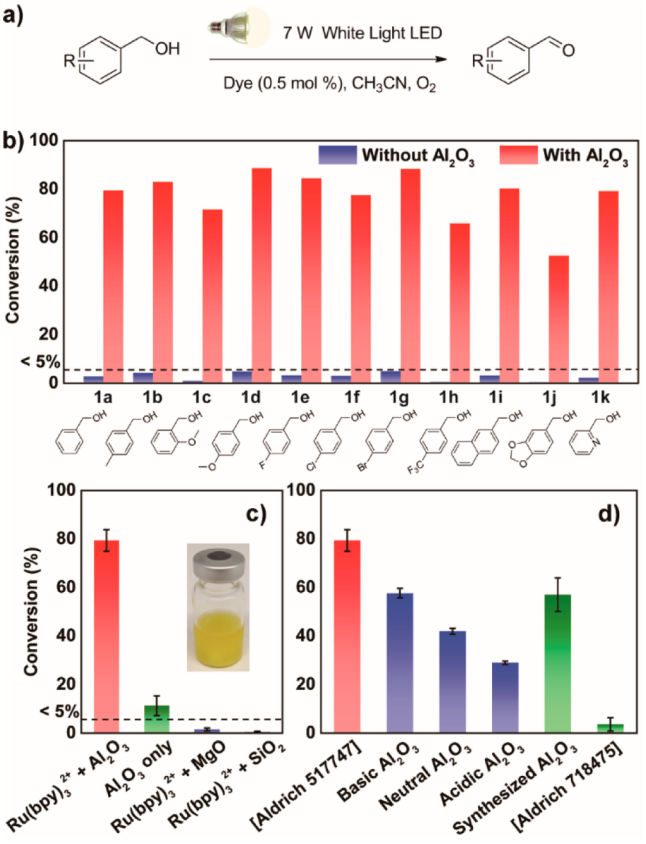

Figure 1. Photocatalytic organic transformation catalyzed by the Al_2O_3 and dye surface complex system. (a) Visible-light-driven oxidation of benzyl alcohol to aldehyde with O_2. (b) Conversion of different benzyl alcohols by $Ru(bpy)_3^{2+}$ with and without Al_2O_3. (c) Conversion of BnOH with different metal oxides and $Ru(bpy)_3^{2+}$. (d) Extensiveness of the Al_2O_3 and $Ru(bpy)_3^{2+}$ dual surface complex system toward different commercial Al_2O_3 products.

showed that the Al_2O_3 is γ-crystalline (Figure S1a), while HRTEM and SEM revealed that the Al_2O_3 comprises micrometer-sized mesoporous particles (Figures S2a and S3a). Al_2O_3 also boasts a large BET surface area of 332 m^2/g, which is favorable for catalysis (Figure S4a and Table S1). XPS suggests that the Al_2O_3 is free of metal ions; the characteristic peaks for metals commonly used in catalysis, i.e., Ag, Au, Co, Cu, Fe, Mn, Mo, Ni, Ru, and Pd, were not observed (Figure S5). It can be seen from Figure 1b that the simple addition of Al_2O_3 caused a large increase in conversions for all 11 benzyl alcohols (52.5−88.6%, with most over 75.0%), while $Ru(bpy)_3^{2+}$ alone only afforded trace conversions (<5.0%). The addition of Al_2O_3 has increased the turnover number (TON) of benzyl alcohol (BnOH) with respect to $Ru(bpy)_3^{2+}$ by over 30 times (Figure S6a). This discovery is paradoxical to existing paradigms as Al_2O_3 is known as an insulator[38] and tends to play a supporting rather than a central role in photocatalysis.[36,37]

Meanwhile, characterization of the postreaction Al_2O_3 suggests that only the surface of Al_2O_3 was involved in the photocatalytic reaction. The XRD spectra of the postreaction Al_2O_3 showed negligible change in its crystallinity (Figure S1b). On the basis of the SEM and TEM images, there appears to be little change in the morphology of Al_2O_3 (Figures S2b and S3b). Surface adsorption studies confirmed that Al_2O_3 retained its mesoporous structure, but the BET surface area was somewhat reduced, which may be due to the centrifugation of the Al_2O_3 during its separation from the reaction mixture (Figure S4b and Table S1). No significant differences were observed in the XPS spectra of Al_2O_3 after reaction (Figure S7). This implies that Al_2O_3 was not consumed during the reaction to generate active catalytic species.

The addition of Al_2O_3 to $Ru(bpy)_3^{2+}$ could also significantly improve the selective oxidation of phenol **2a** to cyclohexa-2 5-dien-1-one **2′a** (from 0 to 14.5%, Table S2). Although some extent of hydroquinone **2b** oxidation to quinone **2′b** could be achieved with $Ru(bpy)_3^{2+}$ alone (21.0%), the inclusion of Al_2O_3 could lead to a dramatic increase in yield (61.3%).[54] However, for aliphatic alcohols such as butanol **2c**, pentanol **2d**, and cyclohexanol **2e** (from 0.130−0.243% to 4.88−8.42%, Table S2), only a small improvement in yield was observed. This may be because the low acidity of the α proton renders it less favorable toward the formation of H_2O_2. For furfuryl alcohol **2f**, although the conversion was 99.3%, there was no selectivity for furfural **2′f** (Table S2). The combined Al_2O_3−$Ru(bpy)_3^{2+}$ surface complex system also showed improved conversion in the hydroxylation of phenylboronic acid **3a** to phenol **3′a** (from 14.6 to 96.0%) but not the epoxidation of styrene **3b** (Table S3). The oxidations of benzylamine **3c** and thioanisole **3d** to imine **3′c** and sulfoxide **3′d** were easily able to proceed to completion with $Ru(bpy)_3^{2+}$ only; hence, the addition of Al_2O_3 would not be necessary. Due to the limited scope of this article, only the mechanism of BnOH oxidation will be examined in detail.

It is interesting that the phenomenon appears to be exclusive to Al_2O_3; with other metal oxides such as SiO_2 and MgO, negligible BnOH conversions were observed (Figure 1c). The TON achieved with Al_2O_3 was >50 times higher than that with SiO_2 and MgO (Figure S6a). The initial rate of conversion and turnover frequency (TOF) were relatively high with Al_2O_3, but decreased due to the decreasing concentration of BnOH available for reaction and the formation of hydroxyl groups on the Al_2O_3 surface[40] when the byproduct H_2O_2[55−57] decomposes to H_2O (Figures S6b,c and S8).[58] Control studies revealed that negligible BnOH conversion occurred in the dark and under N_2 (Figure S9a), which indicated that (1) the reaction proceeds via a photocatalytic pathway and (2) O_2 is essential for the transformation of BnOH, suggesting that O_2 serves as a sacrificial electron acceptor that receives 2 electrons and 2 protons from BnOH to form benzaldehyde. The BnOH conversion generally increased with the amount of Al_2O_3 used, but the extent of increment becomes less significant for larger amounts of Al_2O_3 (Figure S9b). Figure 1d showed that the phenomenon applies to other commercial Al_2O_3 and Al_2O_3 synthesized via solid state reaction but not to the non-mesoporous commercial Al_2O_3 [Aldrich 718475]. It can also be observed that the basic Al_2O_3 [Alfa Aesar 11503] showed higher conversion compared to the neutral [Alfa Aesar 11502] and acidic Al_2O_3 [Alfa Aesar 11501], which suggests the importance of Brønsted basicity in enabling the reaction. The characterizations of the aforementioned Al_2O_3 samples can be found in Figures S1−S4 and Table S1.

This phenomenon can also be extended to a large variety of dyes with different moieties, i.e., naphthalene, anthracene, porphyrin, and perylene. While none of the dyes were able to oxidize BnOH in the absence of Al_2O_3, most were able to achieve some BnOH conversion when Al_2O_3 was added (Figure

DOI: 10.1021/jacs.6b09934
J. Am. Chem. Soc. 2017, 139, 269−276

2). A positive relationship can be observed between the dye excitation wavelengths (Figure S10d) and extent of BnOH

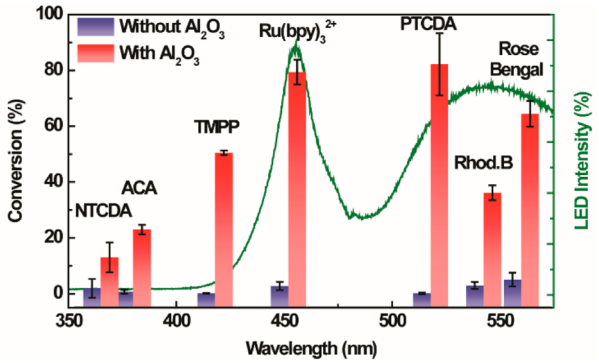

Figure 2. Extensiveness of the Al_2O_3 and dye surface complex system toward dyes of different moieties.

conversion. $Ru(bpy)_3^{2+}$ and perylene-3,4,9,10-tetracarboxylic dianhydride (PTCDA), with excitation wavelengths between 450 and 550 nm, showed extremely high conversions of 79.4(±4.4)% and 82.2(±11.1)%, respectively. Commercial dyes such as Rose Bengal and Rhodamine B were also able to effect significant conversions of 64.5(±4.6)% and 36.2(±2.6)%, respectively, but their lack of stability undermined their photocatalytic activity. 9-Anthracenecarboxylic acid (ACA) and 1,4,5,8-naphthalenetetracarboxylic dianhydride (NTCDA), with absorbance peaks in the range of 300−400 nm far from the LED wavelengths, yielded a low conversion of 23.0(±1.7)% and 13.1(±5.3)%, respectively. However, when the light source was switched to one with a wavelength range that is suitable for absorption by the ACA (350−750 nm), the combined Al_2O_3−ACA surface complex system was able to effect a significant degree of conversion, i.e., 78.0% in 2 h (Figure S11a). It must be noted that ACA by itself was only able to achieve a low conversion of 27.3%. This suggests that different wavelengths of light can be accessed by the Al_2O_3−dye surface complex system by merely selecting a dye with an appropriate excitation wavelength. For instance, the use of $Ru(bpy)_3^{2+}$ with Al_2O_3 showed higher conversion than Degussa P25 under the 450−750 nm wavelength range, and the use of PTCDA with Al_2O_3 showed higher conversion under the 490−750 nm wavelength range (Figure S11b).

3.1. Decrease of BnOH Oxidation Potential Due to Benzylic O−H Dissociation. The success of the Al_2O_3−$Ru(bpy)_3^{2+}$ photocatalytic system and the negligible activity of the individual $Ru(bpy)_3^{2+}$ can be explained by the decrease of the BnOH oxidation potential through surface complexation with Al_2O_3. In Figure 1b, 2-methoxybenzyl alcohol **1c** (71.6%) showed a lower conversion relative to 4-methoxybenzyl alcohol **1d** (88.6%), as the methoxy group in the ortho position provides greater steric hindrance around the O−H group. The decrease in conversion with increasing amounts of acetic acid added (Figure S12a) suggests that the Brønsted base sites on Al_2O_3 (Figures S13a,b) are responsible for the surface complexation, as acetic acid would compete with BnOH for chemisorption on Brønsted base sites. Cyclic voltammetry conducted on BnOH in acetonitrile with a bare glassy carbon electrode showed an irreversible BnOH oxidation peak at around +2.0 V vs Ag/AgCl.[35] As the $Ru(bpy)_3^{2+}/Ru(bpy)_3^{3+}$ potential in acetonitrile is +1.29 V vs SCE,[3,13] BnOH cannot be oxidized by $Ru(bpy)_3^{3+}$. However, the use of an Al_2O_3-modified electrode resulted in an additional oxidation feature at around +0.63 V vs Ag/AgCl (Figure 3a), which is within the oxidative

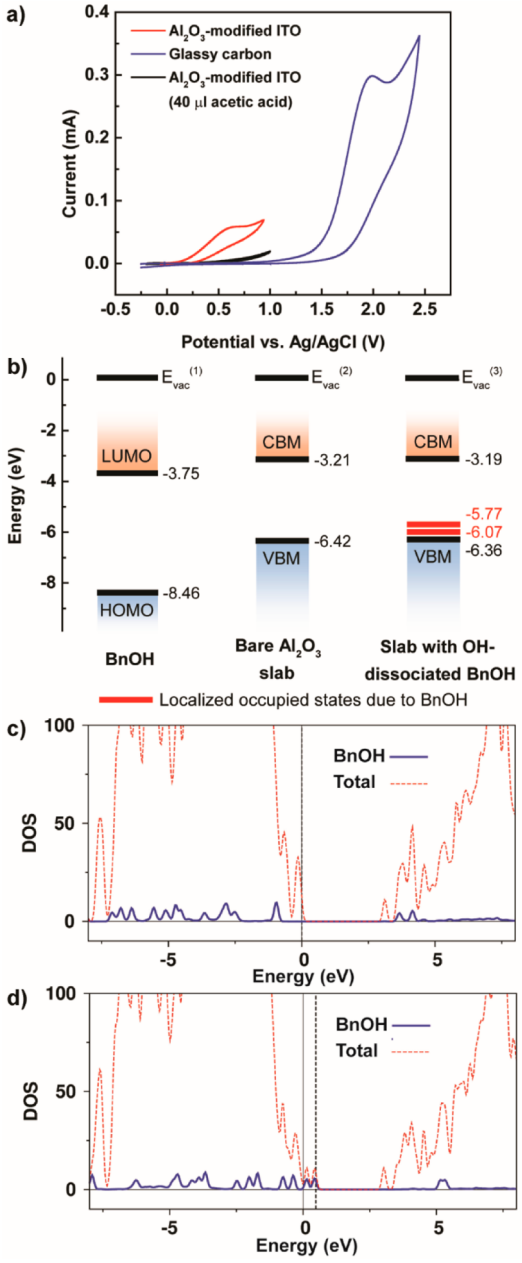

Figure 3. Chemisorption on the surface of Al_2O_3 decreases the oxidation potential of BnOH. (a) Cyclic voltammogram of BnOH with Al_2O_3-modified (red) and bare electrodes (blue) and 40 μL of acetic acid (black). (b) Energy levels of Al_2O_3, free BnOH and the chemisorbed surface complex. (c) DOS of BnOH physically adsorbed to the Al_{III} site and (d) chemisorbed via OH dissociation. The dashed line indicates the formation of localized occupied states just above the VBM of Al_2O_3.

potential of $Ru(bpy)_3^{3+}$. This oxidation feature is suggestive of a chemisorbed BnO−Al_2O_3 surface complex, which is oxidized at the Al_2O_3−bare electrode interface. The BnO−Al_2O_3 surface complex is characterized by a lower oxidation potential and can be easily oxidized by $Ru(bpy)_3^{3+}$ (Figure 4a, step II). No additional oxidation feature was detected for the SiO_2- and MgO-modified electrodes (Figure S15a), while similar oxidation peaks are detected for other BnOH derivatives

DOI: 10.1021/jacs.6b09934
J. Am. Chem. Soc. 2017, 139, 269−276

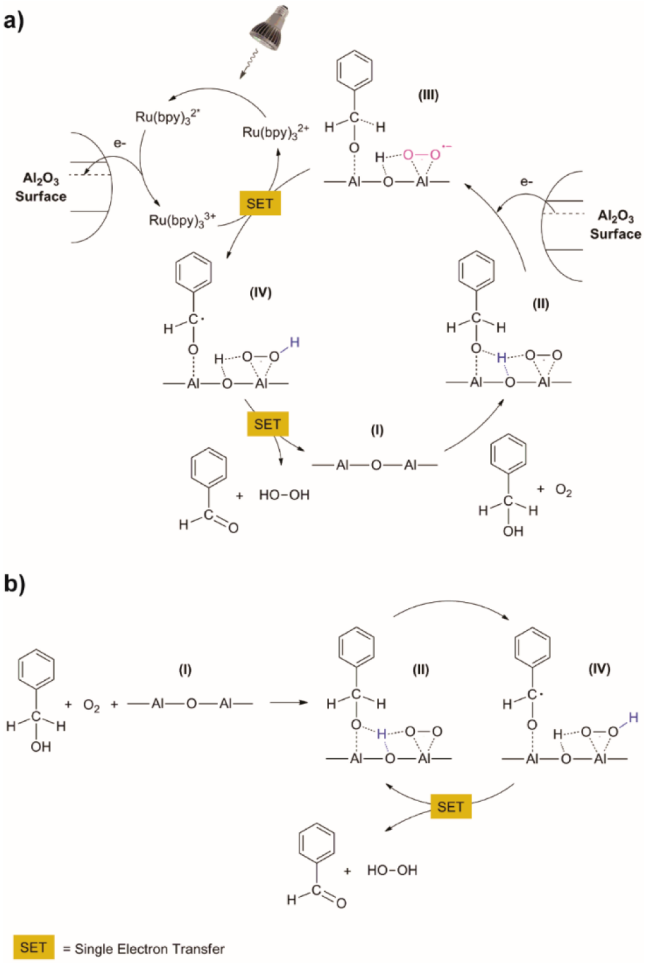

Figure 4. Proposed mechanism of visible-light-driven BnOH oxidation by the Al_2O_3 and $Ru(bpy)_3^{2+}$ surface complex system. (a) Initiation process involving the $Ru(bpy)_3^{2+}$ photosensitizer. (b) Subsequent chain propagation process involving two surface complex intermediates.

(Figure S15b–d). The addition of acetic acid caused a quenching of the oxidation feature at +0.63 V vs Ag/AgCl (Figure 3a), indicating that the BnO–Al_2O_3 surface complexation occurs through O–H deprotonation by the Brønsted base surface sites. As little BnOH conversion occurred when Al_2O_3 was replaced by inorganic bases (Figure S12b), this suggests that surface complexation on Al_2O_3 has a stabilizing effect on the deprotonated BnO^-.

Furthermore, the decrease of BnOH oxidation potential through surface complexation is validated through first-principles calculations on free BnOH and BnOH adsorbed on the most widely exposed plane of the γ-phase Al_2O_3 surface, the (110) facet, based on the Digne model (Figure S16a).[46] The HOMO of the free BnOH molecule was calculated as −8.46 eV (Figure 3b). The DOS diagrams for the adsorption of BnOH onto the Al_{III} site (Figure 3c,d) show that O–H dissociation results in an upward shift in the PDOS of BnOH and the appearance of two additional occupied peaks (the left-hand side of the black dashed line with energy >0 eV). The two peaks correspond to occupied localized states arising from the molecule (Figure S16d), and their energy levels are colored in red in Figure 3b. These occupied states arise as BnOH draws electron density from the surface after O–H dissociation to stabilize its new alkoxide state, which causes it to become electron-rich while creating an electron deficiency in a localized area of the surface. The electron gain by BnOH increases the electron repulsion within the molecule and causes an upward shift in energy level. As the C–H σ-bonds are located at the valence edge, a hole generated on the surface by $Ru(bpy)_3^{3+}$ oxidation and transferred to BnOH would result in the weakening and subsequent cleavage of the C–H bond to form benzaldehyde (Figure 4a, steps III–IV). In this way, Al_2O_3 enables the oxidation of BnOH through the formation of a chemisorbed surface complex that has a lower oxidation potential than that of $Ru(bpy)_3^{2+}/Ru(bpy)_3^{3+}$.

In the previous section, it has been demonstrated that the reaction proceeds via a photocatalytic pathway. However, the high apparent quantum yield of the reaction in the first hour (15.4%, Figure S17) appears to suggest the possibility of a secondary chain propagation pathway (Figure 4b), in which the carbocationic intermediate IV donates an electron to a neighboring chemisorbed BnOH (intermediate II). From Figure S17c, it can be seen that the initial quantum yield of the reaction increases almost proportionally with the amount of BnOH, such that a high value of 69.6% was achieved for 1.0 mmol of BnOH. The combination of two pathways may have enabled the reaction to proceed with high efficacy with a given amount of light energy.

3.2. Electron Transfer from $Ru(bpy)_3^{2+}$ Due to Activation of O_2. As a control experiment to confirm the interaction between Al_2O_3 and the photosensitizer, we grafted $Ru(bpy)_3^{2+}$ to the surface of Al_2O_3 through –COOH groups, in

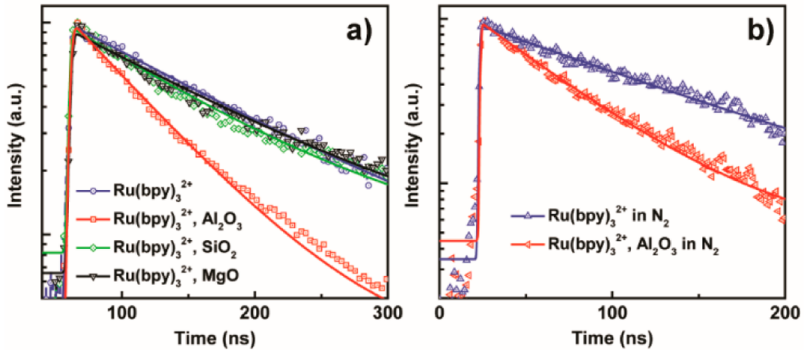

Figure 5. Decay kinetics of TRPL signals of $Ru(bpy)_3^{2+}$ and $Ru(bpy)_3^{2+}$ adsorbed on Al_2O_3, SiO_2, and MgO under (a) ambient and (b) N_2 atmosphere.

DOI: 10.1021/jacs.6b09934
J. Am. Chem. Soc. 2017, 139, 269–276

order to reduce the proximity between the two (Table S4, column [b]). As BnOH conversion is generally greater for the grafted $Ru(bpy)_3^{2+}$ relative to the ungrafted $Ru(bpy)_3^{2+}$, the interaction of the dye with Al_2O_3 appears to be significant for the reaction. To understand the nature of such an interaction, time-resolved photoluminescence (TRPL) spectroscopy was used to study the charge-transfer dynamics between the ungrafted $Ru(bpy)_3^{2+}$ and Al_2O_3. First, $Ru(bpy)_3^{2+}$ was photoexcited using 400 nm laser pulses. The excited species $Ru(bpy)_3^{2+*}$ are generated from the metal-to-ligand charge transfer (MLCT) process[59] and decay exponentially with time, yielding the resultant TRPL signal (Figure 5a). This PL decay arises from a combination of radiative and nonradiative processes: (1) the recombination of charge carriers to regenerate $Ru(bpy)_3^{2+}$ and (2) the loss of an electron to O_2 through electron transfer.

$$Ru(bpy)_3^{2+} \xrightarrow{h\nu} Ru(bpy)_3^{2+*} \rightarrow Ru(bpy)_3^{2+} \quad (1)$$

$$Ru(bpy)_3^{2+} + O_2 \xrightarrow{h\nu} Ru(bpy)_3^{2+*} + O_2 \rightarrow Ru(bpy)_3^{3+} + O_2^- \quad (2)$$

As a similar TRPL lifetime can be observed in the absence of O_2 (Figure 5b and Table 1), the recombination pathway (eq 1)

Table 1. Decay Lifetimes of the Samples Measured under Ambient and N_2 Atmospheres

entry	sample	atmosphere	lifetime (ns)
1	$Ru(bpy)_3^{2+}$	ambient	125 ± 2
2	$Ru(bpy)_3^{2+} + Al_2O_3$	ambient	63 ± 1
3	$Ru(bpy)_3^{2+} + SiO_2$	ambient	105 ± 2
4	$Ru(bpy)_3^{2+} + MgO$	ambient	122 ± 2
5	$Ru(bpy)_3^{2+}$	N_2	115 ± 2
6	$Ru(bpy)_3^{2+} + Al_2O_3$	N_2	55 ± 1

appears to be the dominant process. Although the oxidation potential of O_2 is suitable for receiving electrons from $Ru(bpy)_3^{2+*}$, there appears to be little electron transfer between $Ru(bpy)_3^{2+*}$ and O_2 within the 300 ns time frame in the case of $Ru(bpy)_3^{2+}$ alone. The lack of BnOH conversion with MgO and SiO_2 may also be due to negligible electron transfer from $Ru(bpy)_3^{2+*}$ to MgO or SiO_2, as the lifetimes of $Ru(bpy)_3^{2+*}$ on MgO and SiO_2 are largely similar to that of $Ru(bpy)_3^{2+*}$ alone (Figure 5a and Table 1). There also appears to be no electron transfer between $Ru(bpy)_3^{2+*}$ and BnOH, as no change in the lifetime of $Ru(bpy)_3^{2+*}$ was observed when BnOH was added (Figure S18).

Finally, we examine the case where $Ru(bpy)_3^{2+}$ is adsorbed on Al_2O_3. It can be seen that under both ambient and nitrogen conditions the lifetime of $Ru(bpy)_3^{2+*}$ in the presence of Al_2O_3 is almost half that of $Ru(bpy)_3^{2+*}$ alone. This suggests that in addition to the aforementioned recombination process, there is also a dominant electron transfer process from $Ru(bpy)_3^{2+*}$ to form $Ru(bpy)_3^{3+}$. The idea that an additive or cocatalyst can render a reaction thermodynamically feasible by accepting and transferring electrons has been frequently proposed in literature.[60−62] However, DFT calculations reveal that the CBM of the Al_2O_3 surface is too high at −3.21 eV to receive an electron from $Ru(bpy)_3^{2+*}$. Hence, it is hypothesized that electron transfer may not have occurred directly from $Ru(bpy)_3^{2+*}$ to Al_2O_3, but to a O_2 molecule strongly complexed to the surface of Al_2O_3, which may not have been released in the nitrogen atmosphere (Figure 6a). This hypothesis is consistent with a previous report that O_2 may

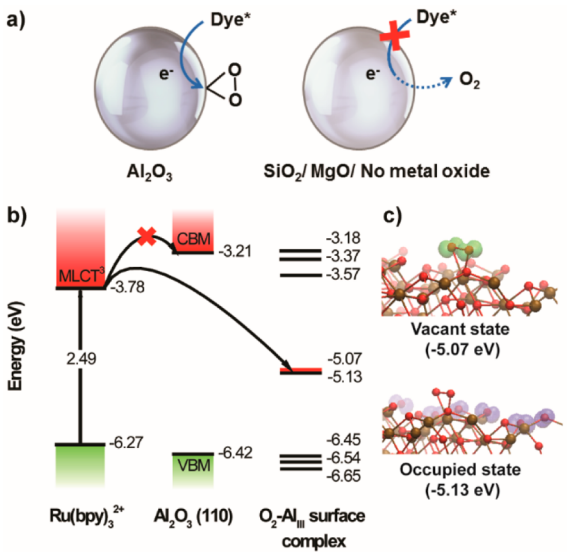

Figure 6. (a) Scheme of proposed electron transfer between dye and O_2. (b) Energy levels of $Ru(bpy)_3^{2+}$, Al_2O_3, and O_2. (c) Occupied and vacant states of the singly occupied π orbital which arose due to O_2 and Al_2O_3 surface complexation.

play a crucial role in the electron transfer processes of organic adsorbates at the Al_2O_3 surface.[63] DFT calculations show that in the gas phase of O_2 the π_x and π_y are half occupied and have the same energy level. However, when O_2 strongly complexed with the Al_{III} site of Al_2O_3, the π_x and π_y become energetically inequivalent and lead to a singly occupied π orbital on the surface. This results in the appearance of a localized vacant band at −5.07 eV (Figure 6b,c), which is suitable for accepting electrons from $Ru(bpy)_3^{2+*}$ to yield superoxide O_2^- (eqs 3 and 4 and Figure 4a, steps II−III).

$$Ru(bpy)_3^{2+} + O_2{-}Al_{III} \xrightarrow{h\nu} Ru(bpy)_3^{2+*} + O_2{-}Al_{III} \quad (3)$$

$$Ru(bpy)_3^{2+*} + O_2{-}Al_{III} \rightarrow Ru(bpy)_3^{3+} + O_2^-{-}Al_{III} \quad (4)$$

The loss of electrons from $Ru(bpy)_3^{2+*}$ would then yield the oxidant species $Ru(bpy)_3^{3+}$, which would drive the reaction forward by removing an electron from the adsorbed BnOH to form an α-carbon radical (Figure 4a, steps III−IV). The overall process is such that with Al_2O_3 and the photoexcited $Ru(bpy)_3^{2+*}$ acting in tandem as a shuttle an electron transfer is enabled from BnOH to O_2. It should be noted that the localized vacant band of the $O_2{-}Al_{III}$ complex at −5.07 eV is also suitable for accepting electrons from the excited states of all dyes used in Figure 2 (Figure S19a), which could account for the efficacy of the Al_2O_3−dye surface complex system.

4. CONCLUSION

We employed the unconventional strategy of utilizing Al_2O_3 surface complexation to modify the oxidation potential of organic reactants, which would enable the oxidation of organic reactants with high oxidation potentials inaccessible to the unassisted photocatalyst. This has been successfully demonstrated through the photocatalytic oxidation of benzyl alcohols to benzaldehydes. High conversion and selectivity can be

DOI: 10.1021/jacs.6b09934
J. Am. Chem. Soc. 2017, 139, 269−276

achieved with the surface complex systems comprising Al_2O_3 and a variety of dyes, but not with these dyes alone. The formation of the chemisorbed BnO−Al_2O_3 surface complex is attributed to the strong Brønsted base sites on Al_2O_3, which accepts protons from benzylic O−H. This causes a shift in the oxidation potential of BnOH, which enhances the ease of subsequent electron and C−H proton abstraction to form benzaldehyde. The surface complexation of O_2 with Al_2O_3 also activates the adsorbed O_2 for receiving electrons from the photoexcited dyes. This discovery may subvert our understanding of the role of Al_2O_3 in photocatalytic reactions. For instance, it may be possible for Al_2O_3 to play a role beyond that of a mere support or scaffold in the performance enhancement in solar hydrogen production[64] and dye-sensitized solar cells.[65,66] This discovery brings forth a new methodology of utilizing surface complexation mechanisms between the reactants and earth-abundant materials to effectively achieve a wider range of photoredox reactions.

■ ASSOCIATED CONTENT

Supporting Information

The Supporting Information is available free of charge on the ACS Publications website at DOI: 10.1021/jacs.6b09934.

Experimental procedures, control experiments, DFT calculations, material surface characterizations, and the reaction mechanism (PDF)

■ AUTHOR INFORMATION

Corresponding Authors

*E-mail: hirao@ntu.edu.sg.
*E-mail: chenxd@ntu.edu.sg.

ORCID

Xianjun Lang: 0000-0001-7479-9044
Shuzhou Li: 0000-0002-2159-2602
Xiaodong Chen: 0000-0002-3312-1664

Notes

The authors declare no competing financial interest.

■ ACKNOWLEDGMENTS

We gratefully acknowledge financial support from Singapore Ministry of Education Tier 1 (RG130/14) and the Singapore NRF through the Singapore-Berkeley Research Initiative for Sustainable Energy (SinBeRISE) CREATE Programme. T.C.S. acknowledges the financial support from Singapore Ministry of Education Tier 2 (MOE2013-T2-1-081 and MOE2014-T2-1-044). H.H. is grateful for a Nanyang Assistant Professorship and a JST-PRESTO grant.

■ REFERENCES

(1) Devery, J. J., III; Stephenson, C. R. J. *Nature* **2015**, *519*, 42.
(2) Yoon, T. P.; Ischay, M. A.; Du, J. *Nat. Chem.* **2010**, *2*, 527.
(3) Narayanam, J. M. R.; Stephenson, C. R. J. *Chem. Soc. Rev.* **2011**, *40*, 102.
(4) Maeda, K.; Sahara, G.; Eguchi, M.; Ishitani, O. *ACS Catal.* **2015**, *5*, 1700.
(5) Kuriki, R.; Matsunaga, H.; Nakashima, T.; Wada, K.; Yamakata, A.; Ishitani, O.; Maeda, K. *J. Am. Chem. Soc.* **2016**, *138*, 5159.
(6) Cuthbertson, J. D.; MacMillan, D. W. C. *Nature* **2015**, *519*, 74.
(7) Jin, J.; MacMillan, D. W. C. *Nature* **2015**, *525*, 87.
(8) Zuo, Z.; Ahneman, D. T.; Chu, L.; Terrett, J. A.; Doyle, A. G.; MacMillan, D. W. C. *Science* **2014**, *345*, 437.
(9) Tellis, J. C.; Primer, D. N.; Molander, G. A. *Science* **2014**, *345*, 433.
(10) Shu, X.-z.; Zhang, M.; He, Y.; Frei, H.; Toste, F. D. *J. Am. Chem. Soc.* **2014**, *136*, 5844.
(11) Sahoo, B.; Hopkinson, M. N.; Glorius, F. *J. Am. Chem. Soc.* **2013**, *135*, 5505.
(12) Hopkinson, M. N.; Sahoo, B.; Li, J.-L.; Glorius, F. *Chem. - Eur. J.* **2014**, *20*, 3874.
(13) Prier, C. K.; Rankic, D. A.; MacMillan, D. W. C. *Chem. Rev.* **2013**, *113*, 5322.
(14) Vila, C. *ChemCatChem* **2015**, *7*, 1790.
(15) Xie, J.; Shi, S.; Zhang, T.; Mehrkens, N.; Rudolph, M.; Hashmi, A. S. *Angew. Chem., Int. Ed.* **2015**, *54*, 6046.
(16) Noble, A.; McCarver, S. J.; MacMillan, D. W. *J. Am. Chem. Soc.* **2015**, *137*, 624.
(17) Primer, D. N.; Karakaya, I.; Tellis, J. C.; Molander, G. A. *J. Am. Chem. Soc.* **2015**, *137*, 2195.
(18) Wang, F.; Li, C.; Chen, H.; Jiang, R.; Sun, L. D.; Li, Q.; Wang, J.; Yu, J. C.; Yan, C. H. *J. Am. Chem. Soc.* **2013**, *135*, 5588.
(19) Chu, L.; Lipshultz, J. M.; MacMillan, D. W. *Angew. Chem., Int. Ed.* **2015**, *54*, 7929.
(20) Higashimoto, S.; Kitao, N.; Yoshida, N.; Sakura, T.; Azuma, M.; Ohue, H.; Sakata, Y. *J. Catal.* **2009**, *266*, 279.
(21) Ohkubo, K.; Suga, K.; Fukuzumi, S. *Chem. Commun.* **2006**, 2018.
(22) Tanaka, A.; Hashimoto, K.; Kominami, H. *J. Am. Chem. Soc.* **2012**, *134*, 14526.
(23) Chen, L.; Peng, Y.; Wang, H.; Gu, Z.; Duan, C. *Chem. Commun.* **2014**, *50*, 8651.
(24) Lang, X.; Leow, W. R.; Zhao, J.; Chen, X. *Chem. Sci.* **2015**, *6*, 1075.
(25) Lang, X.; Zhao, J.; Chen, X. *Angew. Chem., Int. Ed.* **2016**, *55*, 4697.
(26) Zhang, M.; Chen, C.; Ma, W.; Zhao, J. *Angew. Chem., Int. Ed.* **2008**, *47*, 9730.
(27) Sun, M.; Zhang, J.; Putaj, P.; Caps, V.; Lefebvre, F.; Pelletier, J.; Basset, J.-M. *Chem. Rev.* **2014**, *114*, 981.
(28) Beller, M. *Adv. Synth. Catal.* **2004**, *346*, 107.
(29) Largeron, M.; Fleury, M. B. *Science* **2013**, *339*, 43.
(30) Largeron, M.; Fleury, M. B. *Angew. Chem., Int. Ed.* **2012**, *51*, 5409.
(31) Lang, X.; Chen, X.; Zhao, J. *Chem. Soc. Rev.* **2014**, *43*, 473.
(32) Shishido, T.; Miyatake, T.; Teramura, K.; Hitomi, Y.; Yamashita, H.; Tanaka, T. *J. Phys. Chem. C* **2009**, *113*, 18713.
(33) Nagib, D. A.; Scott, M. E.; MacMillan, D. W. C. *J. Am. Chem. Soc.* **2009**, *131*, 10875.
(34) Stevenson, S. M.; Shores, M. P.; Ferreira, E. M. *Angew. Chem., Int. Ed.* **2015**, *54*, 6506.
(35) Cano-Yelo, H.; Deronzier, A. *Tetrahedron Lett.* **1984**, *25*, 5517.
(36) Kim, W.; Tachikawa, T.; Majima, T.; Choi, W. *J. Phys. Chem. C* **2009**, *113*, 10603.
(37) Canlas, C. P.; Lu, J.; Ray, N. A.; Grosso-Giordano, N. A.; Lee, S.; Elam, J. W.; Winans, R. E.; Van Duyne, R. P.; Stair, P. C.; Notestein, J. M. *Nat. Chem.* **2012**, *4*, 1030.
(38) Ealet, B.; Elyakhloufi, M. H.; Gillet, E.; Ricci, M. *Thin Solid Films* **1994**, *250*, 92.
(39) Shimizu, K.-i.; Sugino, K.; Sawabe, K.; Satsuma, A. *Chem. - Eur. J.* **2009**, *15*, 2341.
(40) Trueba, M.; Trasatti, S. P. *Eur. J. Inorg. Chem.* **2005**, *2005*, 3393.
(41) Torres Galvis, H. M.; Bitter, J. H.; Khare, C. B.; Ruitenbeek, M.; Dugulan, A. I.; de Jong, K. P. *Science* **2012**, *335*, 835.
(42) Lu, J.; Fu, B.; Kung, M. C.; Xiao, G.; Elam, J. W.; Kung, H. H.; Stair, P. C. *Science* **2012**, *335*, 1205.
(43) Korhonen, S. T.; Beale, A. M.; Newton, M. A.; Weckhuysen, B. M. *J. Phys. Chem. C* **2011**, *115*, 885.
(44) Thibault-Starzyk, F.; Seguin, E.; Thomas, S.; Daturi, M.; Arnolds, H.; King, D. A. *Science* **2009**, *324*, 1048.
(45) Teramura, K.; Tanaka, T.; Yamamoto, T.; Funabiki, T. *J. Mol. Catal. A: Chem.* **2001**, *165*, 299.

DOI: 10.1021/jacs.6b09934
J. Am. Chem. Soc. 2017, 139, 269−276

(46) Digne, M.; Sauteta, P.; Raybaud, P.; Euzenc, P.; Toulhoatd, H. *J. Catal.* **2004**, *226*, 54.
(47) Kresse, G.; Furthmüller, J. *Phys. Rev. B: Condens. Matter Mater. Phys.* **1996**, *54*, 11169.
(48) Kresse, G.; Furthmüller, J. *Comput. Mater. Sci.* **1996**, *6*, 15.
(49) Kresse, G.; Hafner, J. *Phys. Rev. B: Condens. Matter Mater. Phys.* **1993**, *47*, 558.
(50) Kresse, G.; Hafner, J. *Phys. Rev. B: Condens. Matter Mater. Phys.* **1994**, *49*, 14251.
(51) Blöchl, P. E. *Phys. Rev. B: Condens. Matter Mater. Phys.* **1994**, *50*, 17953.
(52) Kresse, G.; Joubert, D. *Phys. Rev. B: Condens. Matter Mater. Phys.* **1999**, *59*, 1758.
(53) Perdew, J. P.; Burke, K.; Ernzerhof, M. *Phys. Rev. Lett.* **1996**, *77*, 3865.
(54) Roth, H. G.; Romero, N. A.; Nicewicz, D. A. *Synlett* **2016**, *27*, 714.
(55) Wang, Q.; Zhang, M.; Chen, C.; Ma, W.; Zhao, J. *Angew. Chem., Int. Ed.* **2010**, *49*, 7976.
(56) Liang, S.; Wen, L.; Lin, S.; Bi, J.; Feng, P.; Fu, X.; Wu, L. *Angew. Chem., Int. Ed.* **2014**, *53*, 2951.
(57) Zhang, M.; Wang, Q.; Chen, C.; Zang, L.; Ma, W.; Zhao, J. *Angew. Chem., Int. Ed.* **2009**, *48*, 6081.
(58) Suh, M.; Bagus, P. S.; Pak, S.; Rosynek, M. P.; Lunsford, J. H. *J. Phys. Chem. B* **2000**, *104*, 2736.
(59) Asbury, J. B.; Ellingson, R. J.; Ghosh, H. N.; Ferrere, S.; Nozik, A. J.; Lian, T. *J. Phys. Chem. B* **1999**, *103*, 3110.
(60) Riener, M.; Nicewicz, D. A. *Chem. Sci.* **2013**, *4*, 2625.
(61) Zhang, J.; Chen, J.; Zhang, X.; Lei, X. *J. Org. Chem.* **2014**, *79*, 10682.
(62) Kranz, D. P.; Griesbeck, A. G.; Alle, R.; Perez-Ruiz, R.; Neudörfl, J. M.; Meerholz, K.; Schmalz, H.-G. *Angew. Chem., Int. Ed.* **2012**, *51*, 6000.
(63) Flockhart, B. D.; Scott, J. A. N.; Pink, R. C. *Trans. Faraday Soc.* **1966**, *62*, 730.
(64) Li, F. T.; Liu, S. J.; Xue, Y. B.; Wang, X. J.; Hao, Y. J.; Zhao, J.; Liu, R. H.; Zhao, D. *Chem. - Eur. J.* **2015**, *21*, 10149.
(65) Lee, M. M.; Teuscher, J.; Miyasaka, T.; Murakami, T. N.; Snaith, H. J. *Science* **2012**, *338*, 643.
(66) Carnie, M. J.; Charbonneau, C.; Davies, M. L.; Troughton, J.; Watson, T. M.; Wojciechowski, K.; Snaith, H.; Worsley, D. A. *Chem. Commun.* **2013**, *49*, 7893.

DOI: 10.1021/jacs.6b09934
J. Am. Chem. Soc. 2017, 139, 269−276